

# Real-Time Ultrawideband MIMO Channel Sounding

Seun Sangodoyin\*, Jussi Salmi†, S. Niranjayan\* and Andreas F. Molisch\*

\*University of Southern California, Dept. of Electrical Engineering, Los Angeles, CA, USA

†Aalto University School of Electrical Engineering, SMARAD CoE, Espoo, Finland

Email:{sangodoy, salmi, niranjay, molisch}@usc.edu

**Abstract**—In this paper, we present a detailed description of the measurement setup and results obtained from a real-time ultrawideband MIMO channel sounding experiment. This channel sounding experiment was designed to perform remote detection of the vital signs of human subjects as well as tracking of mobile targets in an indoor environment. The paper also describes our antenna calibration setup and data processing for the UWB antenna arrays. We show in our analysis that the results from the real-time UWB MIMO channel sounding conveys information of small scale changes in the channel, which are due to the mobile target under observation. Finally, we conclude that the real-time UWB MIMO Channel sounding technique may be used for the localization and surveillance of humans and animals.

## I. INTRODUCTION

Understanding the characteristics of an ultrawideband (UWB) propagation channel is essential to the design and analysis of UWB communication or radar systems. While characterization of *static* channels has been well explored, and measurements of radio channels using vector network analyzers (VNA) are widely available, the real-time characterization of the dynamic spatio-temporal multiple-input-multiple-output (MIMO) radio channel is mostly missing. A significant benefit of such real-time UWB MIMO channel sounding is the capability to achieve improved accuracy for localization and detection purposes as well as precise tracking of mobile targets in a wireless channel. It can, for example, be applied for remote detection of the vital signs of a human subjects.

In this paper, we describe a real-time UWB MIMO channel sounding setup. Also, we describe our antenna calibration setup, employed waveforms and data processing techniques. We also provide examples from a measurement campaign, including detection and tracking of two balls swinging in the channel as well as identifying two breathing persons standing side-by-side at a fixed distance from the Tx and Rx in an indoor environment. Measurements were performed with either a 1 x 8 single-input-multiple-output (SIMO) or an 8 x 8 MIMO antenna array configuration, with line-of-sight (LOS) or non-line-of-sight (NLOS) to either the Tx or Rx. Our analysis capitalizes on the combination of UWB signalling (high range resolution) and the use of multiple antenna elements, which enables estimation of angular parameters of the multipath components (MPCs). Parameters of the MPCs can be extracted using a wideband double-directional channel model [1].

In our previous study [1], we reported a proof of concept measurement campaign of vital sign monitoring, using a non-

real-time setup based on the use of a vector network analyzer (VNA) and virtual antenna arrays. However, due to slow mechanical movement of antennas and long sweep time of the VNA, the system is only applicable under quasi-static channel conditions. In our current measurement, we have used real antenna arrays in which antenna elements at the transmitter and receiver arrays are switched sequentially by RF switches controlled by high speed electronics. This creates Tx-Rx channel combinations for very short durations during which the channel sounding is taking place, hence allowing us to scan through all the Tx-Rx antenna pairs well within the channel coherence time.

The rest of the paper is organized as follows. Section II describes the measurement setup, including the hardware and excitation signals. Section III presents the UWB antenna arrays calibration setup and processing. Section IV details the data post-processing procedure. Section V illustrates results obtain from the measurement campaign while conclusions are drawn in Section VI.

## II. MEASUREMENT SETUP

### A. Hardware

The considered system is designed to measure and characterize the UWB radio propagation channel between two antenna arrays, one transmitting (Tx) and the other receiving (Rx). Measurements provide the transfer function between a transmitting (Tx) antenna array and a receiving (Rx) antenna array as illustrated in Fig. 1a. The details of the measurement hardware are listed in Table I. As shown in Fig. 1a, the heart of the transmit side is an arbitrary waveform generator (AWG), which was used for reproducing the multitone waveforms as well as triggering the antenna arrays and the digital sampling oscilloscope (DSO, a waveform acquisition and display device at the receiver). The AWG was operated in the interleaved mode to utilize maximum available bandwidth. In the interleaved mode, signals from two 10 GS/s digital-to-analog (D/A) channels are offset in time by half of the sampling period and passively combined to reach a higher sampling rate of 20 GS/s. AWG marker channels were configured to send control signals to the DSO and the control circuits of the RF switches controlling the transmit and receive antenna arrays. A pulse generator was used between the AWG and the RF switches in order to ensure good pulse quality and correct logic voltage level for the switch control circuits. Individual control circuits were used to operate the 8-element switched planar monopole

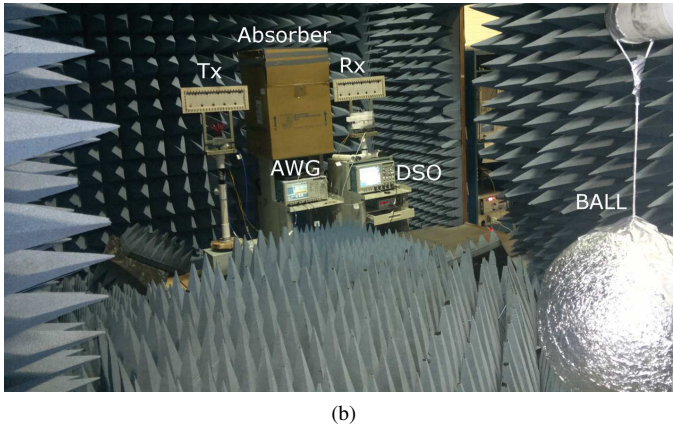
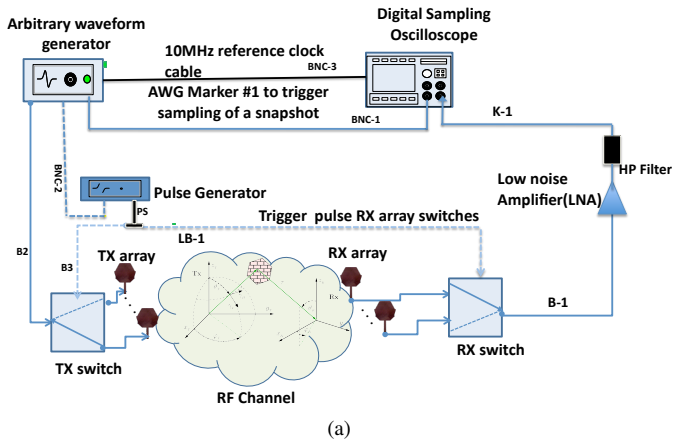


Fig. 1. (a) Real-time UWB MIMO channel sounding setup. (b) MIMO setup in the anechoic chamber.

TABLE I  
HARDWARE USED IN THE UWB MIMO MEASUREMENTS.

Item	Manufacturer	Model No.
AWG	Tektronix	AWG 7102
Pulse generator	HP/Agilent	HP 8110A
DSO	Tektronix	DPO71254B
RF switch(SP8T)	Pulsar Microwave	SW8RD-13
High pass filter	TTE	HC11-1000M
LNA	SCA	SCA04/239

antenna arrays [2], [3] at Tx and Rx in the MIMO setup. In the SIMO configuration, the Tx antenna array was replaced by a high gain UWB horn antenna [4]. The RF chain at the Rx after the array switch was followed by a low noise amplifier (LNA) and a high pass filter (HP), which was used to filter out spikes in the signal introduced by the nonlinear characteristic of the RF switch. The spectral content of these spikes was well below 1 GHz. The amplified and filtered signal was sampled by the DSO at 25 GS/s rate. The AWG and DSO used the same 10 MHz reference clock.

### B. Excitation Signal

We chose to use a multitone waveform as the excitation signal due to several advantages including i) ideally, flat frequency spectrum, ii) design flexibility, iii) controllable crest factor, and iv) high SNR through processing gain. The signal

TABLE II  
UWB MULTITONE SIGNAL PARAMETERS.

Parameter	SIMO/MIMO
Bandwidth, $B$	5.0 GHz
Center frequency, $f_c$	5.0 GHz
Number of multitones, $N_c$	1024/512
Waveform duration, $T = N_c/B$	204.8/102.4 ns
Waveforms per channel, $K$	20/8
Total number of channels, $M$	8/64
Snapshot duration, $T_{ss} = M \cdot K \cdot T$	32.768/52.4288 $\mu$ s
Snapshot repetition rate, $f_{ss}$	40 or 20 1/s

is given by

$$x(t) = \sum_{k=-N_c/2}^{N_c/2-1} \sin(2\pi(f_c + k \cdot \Delta f) \cdot t + \theta_k), \quad (1)$$

where  $f_c$  is the center frequency,  $\Delta f = B/N_c$  the tone (carrier) spacing, and  $\theta_k$  is the phase of the  $k^{\text{th}}$  tone. It is important to adjust the phases  $\theta_k$  in order to minimize the crest factor of the signal<sup>1</sup>. There are several ways to optimize  $\theta_k$ , see e.g. discussion in [5]. The crest factor is reduced in order to maximize the average transmitted power while ensuring that components in the signal's path operate in their linear regions. However, an acceptable crest factor level (about 6 dB) can be easily obtained with Newman phases. With a slight modification of the description in [6], we obtain the phases as

$$\theta_k = \frac{(\pi \cdot k)^2}{N_c/2}. \quad (2)$$

The waveform parameters are listed in Table II. The employed signal occupies the frequency range from 2.5 GHz to 7.5 GHz ( $B = 5$  GHz), covering the useful range of the planar monopole antenna arrays. For SIMO (MIMO) measurements  $N_c = 1024$  (512) carriers were utilized, which results in waveform duration of  $T = N_c/B = 204.8$  ns (102.4 ns) to ensure the orthogonality of the multitone signal. The UWB channel for each antenna pair was measured for  $K = 20$  (8) consecutive waveforms in order to obtain processing gain. Since the DSO buffer was limited by maximum of  $200 \cdot 10^6$  samples, we decided to use different number of subcarriers  $N_c$  and waveform repetitions  $K$  for SIMO and MIMO configurations so as to ensure sufficient measurement duration. Furthermore, the repetition rate of the full MIMO measurement, also called as snapshot, was varied between 20 and 40 snapshots per second to trade-off between the total measurement length vs. capturing the time variation of the channel.

### III. ANTENNA ARRAY CALIBRATION

In order to obtain a coherent characterization of the antenna arrays, an antenna calibration was performed in an RF shielded anechoic chamber (30 x 15 x 15 ft). Modeling the radiation characteristics of the antenna arrays allows angular resolvability of multipath components (MPC), and yields significant focusing gain during data post-processing.

<sup>1</sup>For  $\theta_k = 0$  and  $N_c = 1000$  the crest factor (in dB) would be given by  $10 \log_{10}(2N_c) = 33$  dB.

TABLE III  
ANTENNA ARRAY CALIBRATION PARAMETERS.

Parameter	Rx co-pol(V)	Rx cross-pol(H)
Angular step (degrees)	3°	4°
Number of frequency samples	401	201

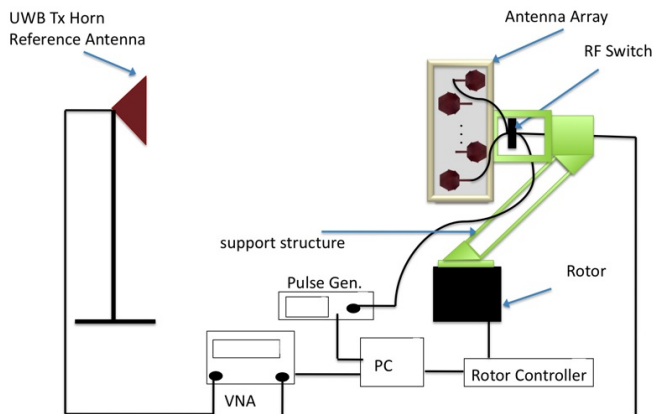


Fig. 2. Antenna array calibration setup.

### A. Hardware Setup

For the antenna calibration, a custom setup was built such that the antenna array was attached to a mounting arm placed on a dual-axes azimuth/elevation rotor (OrbitFR AL-4370-1) operated with a rotor controller (OrbitFR AL-48063-C). The center of the antenna array was aligned with the intersection of azimuth and elevation rotation axes. The UWB horn antenna was used as a reference transmit antenna for the *co/cross*-polarization (vertical/horizontal) measurements. For each array orientation the  $S_{21}$  parameter between the reference antenna and each antenna element was measured over the frequency range of interest using a VNA (Agilent 8720ET). The HP 8110A pulse generator was used for triggering the array switch. All equipment were connected to a PC and controlled by a Labview script. The calibration setup is shown in Fig. 2 while Table III shows all calibration parameters for Rx1 antenna array. The frequency points for calibrating the *co*-polarization of the Rx array were 401 points in the 2–10 GHz range, while the elevation and azimuth angles range from  $-180^\circ$  to  $180^\circ$  and  $-90^\circ$  to  $90^\circ$  at 3 degree increments each. For the Tx array *co*-polarization, as well as both *cross*-polarization measurements, 201 frequency points over the 2–10 GHz bandwidth were used while the angular separation was increased to 4 degrees.

### B. Processing the Antenna Array Calibration Data

In order to use the calibrations for analyzing the measurements, the following steps are necessary:

- Obtaining a, preferably differentiable, description of the antenna array that allows modeling of the antenna responses w.r.t. arbitrary direction of arrival/departure. Potential candidates for achieving this include the 2D-Fourier transform based effective aperture distribution

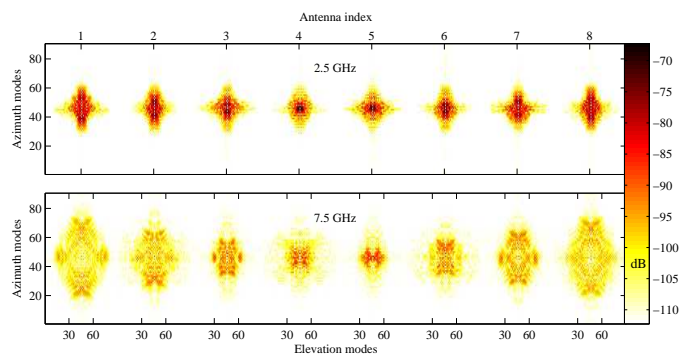


Fig. 3. EADF of the 8 antenna elements at 2.5 and 7.5 GHz. The support area grows with both with frequency as well as the distance of the antenna from the array center.

function (EADF) [7] or spherical wave modeling [8].

- Interpolating the description to match the multitone frequencies. An elegant way to perform this is by taking the inverse Fourier transform over frequency, and zero-padding the signal to a length  $T_{ZP}$  equivalent to the frequency spacing  $\Delta f \approx 1/T_{ZP}$  used in the measurements.

An example of the obtained EADFs for the main (vertical) polarization of the 8-element UWB Tx array (see Fig. 1b) is given in Fig. 3. It can be observed that the required support (number of coefficients) grows with both the frequency and the distance of the antenna from the array center. It should be mentioned that the array calibrations were obtained with measurements at 5.3 meters distance, which is not yet in the far field of the furthest elements at 7.5 GHz. For the EADF model of the array used in this paper we did not compensate for this to obtain a proper far-field model. On the other hand, the propagation measurements were not conducted in far-field conditions either. Thus the results based on this EADF model for the array should be interpreted with some caution. In the future we intend to model the array using spherical harmonic decomposition [8], which enables modeling of the array response at any given distance - even in the near field.

## IV. DATA POST-PROCESSING

The data stored by the DSO is processed offline in order to extract the frequency response of the UWB MIMO radio channel at the multitone frequencies. First, a discrete Fourier transformation (DFT) over the  $K - 1$  waveforms measured per each channel (one lost due to array switching) is performed, and the frequency domain samples at the multitone frequencies are picked as every  $(K - 1)^{\text{th}}$  sample in the frequency range of interest. Fig. 4 shows an example of the power spectrum of the received data, averaged over the eight channels from a SIMO measurement. An estimate of the UWB channel transfer function  $\hat{H}(f)$  at the multitone frequencies is obtained by correlating the samples  $Y(f)$  at the multitone frequencies with a reference signal  $X_{ref}(f)$ , obtained from a measurement where the signal produced by the AWG was sampled by the DSO through a short cable connection. Furthermore, a VNA calibration for the Tx and Rx RF-chains, including all cables,

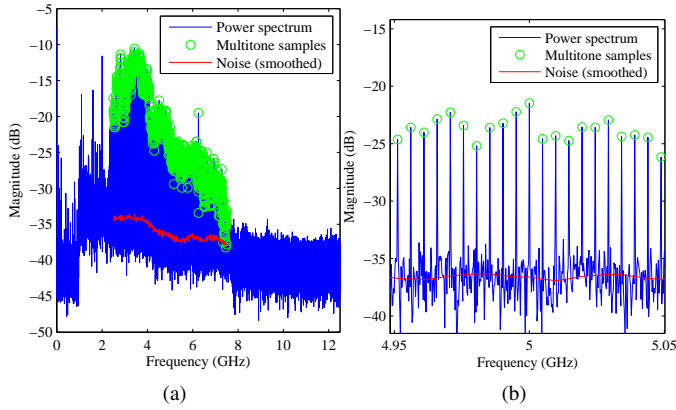


Fig. 4. (a) Spectrum of the received signal (the absolute scale is not meaningful). (b) Zoomed around center frequency.

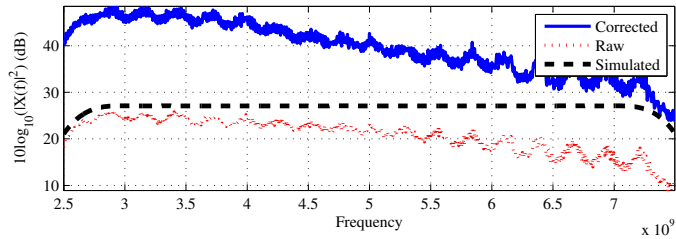


Fig. 5. Comparison of measured (before and after RF-chain correction) and simulated reference signal spectrum.

connectors, LNA and the HP-filter was performed, and the response is included in the reference signal. Fig. 5 shows the spectrum of the reference waveform. Figures 4a and 5 reveal a significant variation in the signal and noise levels over the wide range of frequencies, hence the least squares estimate  $\hat{H}_{LS}(f) = Y_{MT}(f)/X_{ref}(f)$  suffers from noise enhancement in low SNR measurements. The variation of the signal and noise levels over the wide frequency range can be compensated by employing a minimum mean square error (MMSE) type of solution in the correlator, given by

$$\hat{H}(f)_{MMSE} = \frac{X_{ref}(f)^* \cdot Y(f)}{|X_{ref}(f)|^2 + c \cdot \hat{\sigma}_N^2(f)}, \quad (3)$$

where  $\hat{\sigma}_N^2(f)$  is the noise power, see Fig. 4, estimated from the power spectrum values falling between the multitone frequency bins. The scaling factor  $c$  is used for matching the signal levels, and is defined as

$$c = \frac{\bar{\sigma}_{ref}^2}{\max\{(\bar{\sigma}_Y^2 - \bar{\sigma}_N^2), \bar{\sigma}_N^2\}}, \quad (4)$$

where  $\bar{\sigma}_i^2, i \in \{ref, Y, N\}$  denotes the average magnitude squared of the reference signal, received signal and noise, respectively. Fig. 6 shows a comparison of the frequency and impulse response magnitudes for the LS and MMSE correlators for a low SNR MIMO measurement. It can be observed that the MMSE approach provides significantly better SNR.

Note that the obtained channel transfer functions still contain the influence of the antenna arrays and their respective

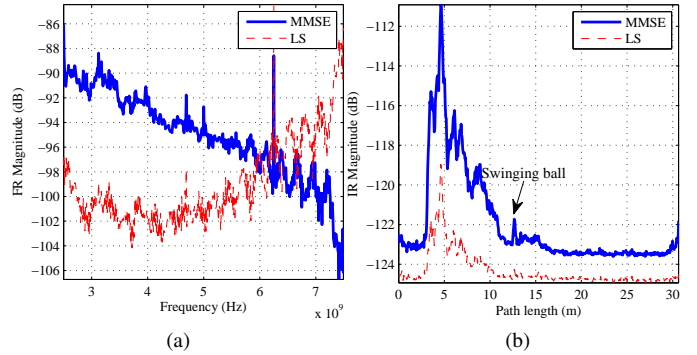


Fig. 6. Comparison of MMSE and LS correlators for a MIMO measurement. Plots show the average over 64 channels and 190 snapshots. (a) Magnitude of the frequency response. (b) Power delay profile.

switches and cabling. However, array calibrations are available and are used for geometry-based parametric analysis of the measurements [9], so that the true responses of the arrays and the switches are accounted for while angular-delay beamforming techniques are implemented to obtain results shown in Section V.

## V. RESULTS

The first example from the real-time UWB MIMO channel sounding measurement campaign illustrates a measurement of two oscillating aluminum foil covered basketballs that are swinging in mid-air at about 2 meters distance from the antennas, see Fig. 7. The oscillatory movement of the balls is clearly visible in the power-delay profile (PDP) in Fig. 8a. Also, we are able to resolve the power-angular-delay profile (PADP) of the oscillating balls averaged over snapshots as shown in Fig. 8b, where the Rx azimuth angle is defined w.r.t. the broadside direction of the array, see Fig. 7.

Fig. 9 shows PDP and PADP views from a measurement where two persons were breathing and standing still side by side at about 5 and 6 meters in front of the measurement setup. The figures also indicate assumed sources of reflection. The resolution of the angular focused PDP plots suffers from the plane-wave assumption of the antenna array model, and the interpretation is difficult also due to the fact that reflections from human subjects are far from that of a point source.

## VI. CONCLUSION

We have successfully performed a real-time UWB MIMO measurement campaign to monitor movement and vital signs. In this paper, we have provided a thorough description of the measurement setup, employed waveforms and data post-processing. Also, we described our antenna calibration setup and data processing for the switched 8-element planar monopole UWB arrays. We also provided analysis of the results of our measurements including that of two balls swinging in a LOS scenario in the channel as well as two human subjects breathing. Our measurement results allow a better understanding of the characteristic of mobile targets in a channel. We conclude that our real-time UWB MIMO channel

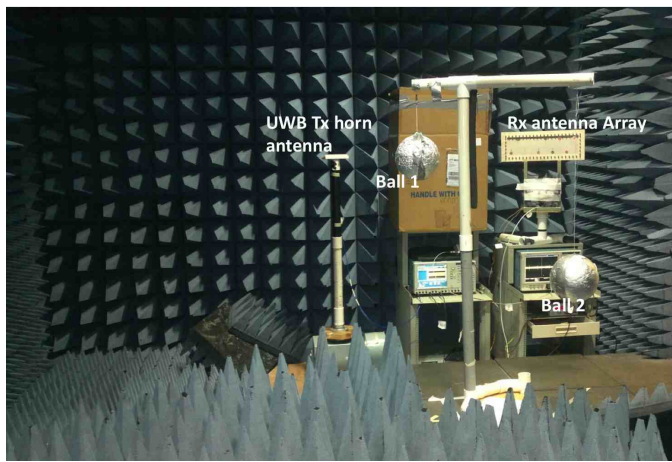


Fig. 7. Two balls Oscillating in the channel with a SIMO setup in LOS scenario.

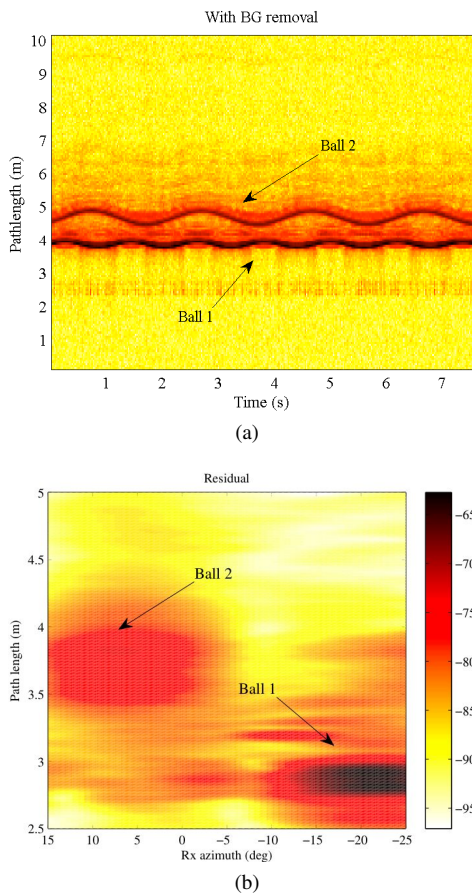


Fig. 8. (a) PDP over time after background removal for SIMO measurement of two oscillating balls.(b)PADP averaged over measurement duration,focused on the region of interest

sounding setup and data processing techniques may be used for the localization and surveillance of humans and animals.

#### ACKNOWLEDGMENT

The authors would like to thank Prof. Hossein Hashemi for providing the DSO, Dr. Xuesong Yang for designing the

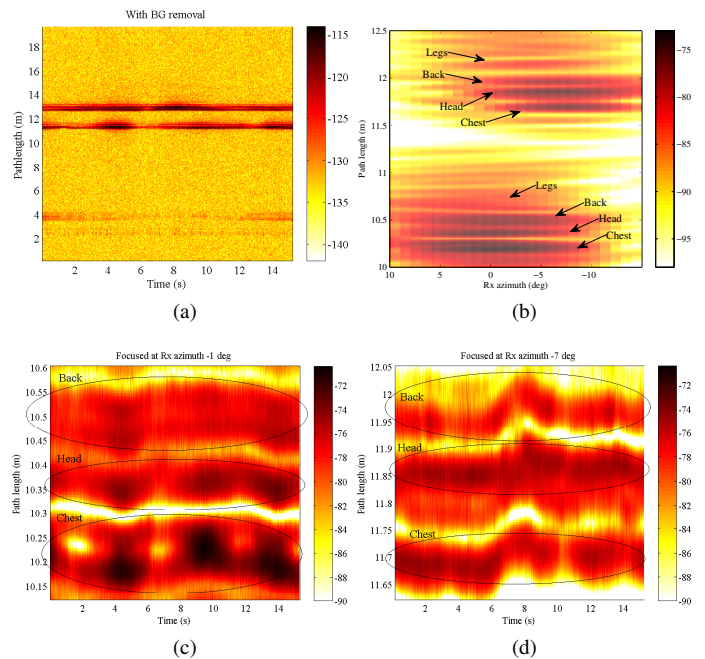


Fig. 9. Results from a SIMO measurement with two persons breathing and standing still. (a) PDP over time after background removal. (b) PADP averaged over measurement duration, focused on the region of interest. (c) PDP over time, focused on the first person by Rx beamforming. (d) PDP focused on the second person.

antennas, Dr. Andreas Richter for insightful discussions as well as Ahmad Golmohammadi and Rui Wang for their help with the antenna calibration.

#### REFERENCES

- [1] J. Salmi and A. F. Molisch, "Propagation parameter estimation, modeling and measurements for ultrawideband MIMO radar," *IEEE Transactions on Antennas and Propagation*, vol. 59, no. 11, pp. 4257–4267, Nov. 2011.
- [2] X.-S. Yang, K. T. Ng, S. H. Yeung, and K. F. Man, "Jumping genes multiobjective optimization scheme for planar monopole ultrawideband antenna," *IEEE Transactions on Antennas and Propagation*, vol. 56, pp. 3659–3666, Dec. 2008.
- [3] X.-S. Yang, J. Salmi, A. F. Molisch, S.-G. Qiu, and B.-Z. Wang, "Trapezoidal monopole antenna and array for UWB-MIMO applications," in *submitted to International Conference on Microwave and Millimeter Wave Technology (ICMMT 2012)*, vol. 6, Shenzhen, China, May 2012.
- [4] T. Lewis, "An ultrawideband digital signal design with power spectral density constraints," Ph. D. dissertation, University of Southern California, Los Angeles CA, USA, 2010.
- [5] M. Friese, "Multitone signals with low crest factor," *IEEE Transactions on Communications*, vol. 45, no. 10, pp. 1338–1344, Oct. 1997.
- [6] S. Boyd, "Multitone signals with low crest factor," *IEEE Transactions on Circuits and Systems*, vol. 33, no. 10, pp. 1018–1022, Oct. 1986.
- [7] M. Landmann, A. Richter, and R. S. Thomä, "DOA resolution limits in MIMO channel sounding," in *International Symposium on Antennas and Propagation and USNC/URSI National Radio Science Meeting*, Monterey, CA, Jun. 2004, pp. 1708–1711.
- [8] J. E. Hansen, *Spherical Near-Field Antenna Measurements*. London, UK: Peter Peregrinus Ltd., 1988, 387 p.
- [9] A. Richter, "Estimation of radio channel parameters: Models and algorithms," Ph. D. dissertation, Technische Universität Ilmenau, Ilmenau, Germany, 2005. [Online]. Available: [www.db-thueringen.de](http://www.db-thueringen.de)